A Well-Shaped Bipolar Outflow Shel

Taoling Xie[1,2]

Paul F. Goldsmith[1]

Nimesh Patel[1]

[1] Five College Radio Astronomy Observatory

Department of Physics and Astronomy

University of Massachusetts

Amherst, MA 01003

Radio/Submm Radio Astronomy Group

c/o S 69-506

JPL/CAltech

Pasadena, CA 91109

Submitted to Astrophysical Journal (*Letters*)

Received

Abstract

We report in this letter the results of a study of the massive bipolar outflow in the central region of the giant molecular cloud Monoceros R2. We find in our $CO\ J = 1 - O$ maps an "eggplant-shaped", thin bipolar outflow shell which outlines the extended blue lobe of the bipolar outflow. The projected length and width of the shell arc about 5.7 pc and 2.5 pc respectively, and the averaged projected thickness of the shell is estimated to be 0.3 pc. The shape of this thin shell and the mass distribution of the blue-shifted outflowing gas as a function of velocity can be satisfactorily accounted for quantitatively within the framework of the Shu *et* al shell model with radially directed wind. The outflow shell's symmetry axis is inclined by $\sim 70°$ with respect to the line of sight. We suggest that the coincident blue- and red-shifted emission and the bending of the red-shifted lobe are the result of the red-shifted shell being compressed, rather than having a second bipolar outflow aligned roughly perpendicular to the axis of the first bipolar outflow.

Subject headings:

1 Introduction

Since the discovery of the first molecular bipolar outflow associated with young stellar objects more than a decade ago (Snell, Loren and Plambeck 1980), extensive observational and theoretical studies have been undertaken. At present, the bipolar outflow phenomenon seems to be one of the relatively best studied phenomena associated with star formation (cf. Bally & Lada 19S3; Lada 1985; Snell 1987; Shu, Adams & Lizano 1987; Bally and Lane 1991). However, outflow research is still at a stage where phenomenological models remain useful tools for improving our understanding about this physical process. in particular, geometrical considerations play a critical role for evaluating models in terms of morphology as well as energetics. Several examples are the filled biconical lobe model by Cabrit & Bertout (1 986; 1990); the shell model by Moriarty-Schieven (1988) and Moriarty-Schieven & Snell (1988); the thin paraboloidal shell model by Meyers-Rice & Lada (1991) and the simple yet powerful shell model by Shu *et al* (1991, hereafter SRLL; see also Masson & Chernin 1992, hereafter MC). The model presented by SRLL not only has the potential to explain important characteristics of observed outflows, but also naturally links the bipolar outflow phenomenon with star-forming activity. One basic element in the SRLL mode] is an elongated, thin, closed expanding shell of swept-up ambient gas, driven through momentum conservation by a radially directed stellar wind.

The Mon R2 bipolar outflow (Loren 1981) is by far one of the largest in size and in mass, among the two hundred or so outflows identified (Bally and Lam 1991). Torrelles *et al* (1983) argue that the bipolar outflow in Mon R2 is collimate] by a toroid which directs the initially isotropic. stellar wind along polar directions. Wolf, Lada & Bally (1990) and h4cyers-Rice & Lada (1991) have presented detailed observational studies of the Mon R2 outflow. Although they discuss evidence for the existence of thin shell, they do not find limb-brightened shells in their spatial maps. The outflowing gas appears to have several components, whit]] Meyers-Rice & Lada (1991) explain in terms of the existence of two distinct pairs of bipolar outflows with flow axes almost perpendicular to each other.

In this letter we report an observational project on the the structure of the Mon R2 bipolar outflow, which focuses on the finding of a well-shaped bipolar outflow shell, and compares its spatial shape and structure with the SRLL model.

2 Observations

Observations of the CO $J = 1 - O$ transition in Mon R2 were made using the QUARRY 15-element focal plane array (Erickson *et al* 1992) at the 14 In FCRAO telescope in New Salem, Massachusetts, from 1991 April to l)c-

cember. The mapping was centered on $\alpha(1950)$ = *06'' 05'''22*^{s}, $\delta(1950)$ = –06°22'25", the position of the infrared star cluster in the core of Mon R2 (cf. Beckwith *et al 1976;* Hodapp 1987; A spin & Walther 1990). The spacing of the data is 25" while the FWHM beam size: of the telescope is about *45"* at 115 GHz and 47" at 110 GHz. The main beam efficiency was estimated to be 0.55. A filterbank spectrometer with resolution of 250 kHz (corresponding to a velocity resolution of 0.65 $km\ s^{-1}$ at 115 GHz) was used as the primary spectrometer with *32* channels for each of the 15 receivers. Chopper wheel calibration was used and the data were taken in a position-switching mode with a common reference position at $\alpha(1950) = 06^h11^m00^s$, $\delta(1950) = -04°30'00"$, Because the velocity coverage of the filterbank available with QUARRY at the time the data were taken was only about 20 $km\ s^{-1}$, whit]] can not provide reliable information for the gas at the high - est velocities, wc sampled a strip more than 30 arcminutes long in CO with 30 arcseconds spacing along the outflow axis, using the single-beam receiver system at the 14111 FCRAO telescope. The primary filterbank used had 256 channels each of 100 kHz bandwidth), corresponding to 0.26 $km\ s^{-1}$ resolution at 115 GHz.

Figure 1a presents velocity channel maps for $CO\ J = 1 - O$ emission in the main core region of Mon R2. One striking feature in Figure la is the appearance of an eggplant-shaped thin shell feature (conspicuous in several channel maps with velocity close to 10.5 $km\ s^{-1}$, the centroid velocity of

the c.ore) extending from the (O, O) position to the North-West for about 22 arcmin. Figure 1b presents an overlay of the high velocity gas with the shell seen in the $V_{LSR} = 10.88\ km\ .s^{-1}$ CO channel map. Figure 1b clearly snows that the blue-shifted lobe of the well-known bipolar outflow sits nicely within the boundary of the Shell, posing the immediate possibility that we arc witnessing the limb-brightened thin shell swept up by collimated stellar winds from the central driving source of the bipolar outflow as predicted by outflow models (cf. Snell 1987; SRLL). Figure 2 shows the spatial-velocity (SV) cut along the outflow axis. Following Meyers-Rice & Lada (1991), we identify four lobe features: the extended blue lobe (EBL), the compact blue lobe (CBL), the compact red lobe (CRL) and the extended red lobe (ERL). While the EBL component is elongated towards the Nortll-West, the ERL component appears snort with a "bent" head.

3 The Outflow Shell

3.1 The Model

The SRLL model expresses the shape of the whole, closed outflow shell with an analytical formula, while other models (cf. Moriarty-Schieven & Snell 1988; 1989; Meyers-lticc & Lada 1991). have considered shells with open ends. Figure 3a is a schematic of the model (cross-section in the plane con-

taining the outflow axis and the line of sight, i.e., $\phi = \pi/2$). The basic formulae can be summarized as follows (SRI,],; MC). In a spherical polar coordinate system (r, θ, ϕ), both the stellar winds from the star and the ambient surrounding medium are assumed to have axial symmetry and reflection symmetry about the equatorial plane $(\theta = \pi/2)$. Specifically, the ram pressure force per steradian, $f(\mu)[g\ cm\ S^{-2}\ sr^{-1}]$, of the wind is a function only of $\mu(= cos\theta)$

$$f(\mu) \propto P(\mu), \tag{1}$$

and the density of the ambient material $\rho(r, \mu)[g\ cm^{-3}\ sr^{-1}]$ can be expressed

$$\rho(r, \mu) \propto \frac{Q(\mu)}{r^2}, \tag{2}$$

where $P(\mu)$ and $Q(\mu)$ arc dimensionless functions not specified by SRLL. Onc approach is to let $P(\mu)$ and $Q(\mu)$ have a power-]aw form (MC), $P(\mu) \propto \mu^{\alpha}$ and $Q(\mu) \propto \mu^{-\beta}$. With these simplifications and the further assumptions that the stellar winds move out by sweeping the ambient medium into a thin shell with momentum conservation ("snowplow") and that the net mass flow along the θ direction in the thin shell is negligible, the shell velocity $v_s(\mu)$ along each radial direction $(\theta = constant)$ will be

$$v_s(\mu) = v_0 \mu^{\delta}, \tag{3}$$

where $\delta = (\alpha+\beta)/2$. Since $v_s(\mu)$ is independent of time, the shell will develop self-similarly, $r_s(\mu) = v_s(\mu)t$. The line of sight velocity of the swept-up gas

is

$$v_l = v_s(\mu)(\sin\theta \sin i \sin\phi + \cos\theta \cos i). \quad (4)$$

Figure 3b shows a simple sl)atia.1-velocity diagram along the projected outflow axis ($\phi = \pi/2$) with an inclination angle i, assuming a perfect thin shell without line-broaclming. The swept-up mass in the shell per steradian, $m(\mu)[g\ sr^{-1}]$, can be written as

$$m(\mu) = \frac{dm_0}{dt} t \mu^{(\alpha-\beta)/2} \quad (5)$$

where v_0 and $\frac{dm_0}{dt}$ are the shell velocity and mass loss rate along the polar direction, respectively.

3.2 The Outflow Shell

In order to see whether the model can account for the observed "eggplant" shaped shell and major characteristics of the high velocity gas, it would be ideal if the model parameters α and β could be determined by observational data (MC). This is a challenging task because many physical processes and various projection effects greatly complicate the way the mode] equations relate to the observed physics] quantities. First, the shell in reality is of finite thickness with velocity broadening as a result of turbulence (SRLL, MC), and the emission from the swept-up gas in the shell is expected to show limb-brightening in velocity channel maps, as can be easily demonstrated by

deriving the locus of constant-velocity emission from the swept-up gas. This explains qualitatively why the limb-brightening (outflow shell) only shows up in a few velocity channel maps in Figure 1. As for the shape of the shell, it can be shown that the maximum extents of the outflow shell along and perpendicular to the outflow axis projected on the plane of the, sky are, respectively,

$$W_s = 2v_0 t \frac{(\delta)^{\delta/2}}{(\delta+1)^{(\delta+1)/2}}, \tag{6}$$

and

$$L_s = v_0 t (\cos\theta_t)^{\delta} \sin(i - \theta_t), \tag{7}$$

where $\theta_t = \arctan\left(\frac{(\delta+1)\tan i - ((\delta+1)^2 \tan^2 i + 4\delta)^{1/2}}{2\delta}\right)$ Scc.end, in the plane determined by the line of sight and the outflow axis, the blue-shifted line of sight velocity of the swept-up gas in the shell is maximized at the following positional offset from the outflow center along the outflow axis,

$$\Delta s = v_0 t (\cos\theta_v)^{\delta} \sin(i - \theta_v), \tag{8}$$

and achieves a maximum value,

$$v_{max} = v_0 (\cos\theta_v)^{\delta} \cos(i - \theta_v), \tag{9}$$

where $\theta_v = \arctan\left(\frac{-(\delta+1) + ((\delta+1)^2 + 4\delta \tan^2 i)^{1/2}}{2\delta \tan i}\right)$.

Notice that W_s, L_s, Δs and v_{max} on the left hand sides in equations 6 through 9 are all quantities that can be determined observationally. Specifically, the maximum width W_s and maximum length L_s of the outflow shell are found

to be 22' ($\sim$ 6.2 pc) and 11' ($\sim$ 3 pc) respectively. As and v_{max} can be determined to be about 1 6' ($\sim$ 4.3 pc) and 8 km/s, respectively, from the S-V diagram along the outflow axis. In obtaining the value for v_{max}, we have taken the centroid velocity of the quiescent gas to be V_{LSR} = 11.0 km/s. This is a bit larger than the V_{LSR} velocity of 1().0 – 10.5 km/s revealed by optically-thin tracers (Wolf, Lada & Bally 1990), but given the velocity gradient on the scale of the outflow (Figure 2), 11 km/s seems to be a better reference velocity to use for the EBL component under discussion. Using Equations 6 -9, the four unknowns, v_0, t, δ and i can be obtained numerically, giving v_0 = 17 km/s, δ = 6, i = 74° and t = 3,2 x $10^5 years$. Figure 1c presents an overlay of the modeled constant velocity locus with the velocity channel map at 10.8 km/s. We see that the mode] explains quite well the shape of the observed outflow shell.

To obtain α and β separately, M C suggested the usc of the observed line profile averaged over the whole outflow, and we present here a variation on this approach, in the plane determined by the outflow axis and the line of sight ($\phi = \pi/2$), the column density sampled by the telescope beam $m(v_l)$ [$g\ cm^{-2}$] is related to $m(\mu)$ by

$$m(v_l) = m(\mu)\Delta\Omega = m(\mu)\frac{\cos(i - \Omega)}{r_s^2}, \qquad \text{(lo)}$$

where μ is obtained from Equations 3 and 4 as a function of v_l and i (ϕ = $\pi/2$). It is plausible that the outflow' shell in reality is of finite thickness

ancl velocity broadened due to turbulence. Indeed, the S-V diagram (Figure 2) indicates that the extended blue-shifted emission shows an arm-feature as expected by the model (see Figure 3b), corresponding to little bumps in the line profiles at different positions, which were taken to be evidence for the existence of shell structure (Wolf, Lada & Bally 1990). Similar "bump" features arc also observed in other outflow sources (cf. Bachiller *et* al 1990). If wc assume that the line-width of the bumps is mainly caused by the turbulent motion and the finite thickness of the shell, and the variation of the centroid velocity at different positions cau be effectively described by Equation 4, then wc expect that the integrated intensity of the little bumps as a function of v_l should approximately follow Equation 10. Figure 4 presents the comparison of Eq. 10 with the data. The data points at lower velocity offsets suffer from large uncertainties because the bump features at velocity offsets smaller than 3 km/s arc very much mixed with emission from the ambient gas. For these data points wc have estimated lower and upper limits, as plotted in Figure 4. The data points at velocity offsets higher than 3 km s^{-1} arc mainly subject to statistical noise of the data, which is estimated to be $\sigma = 0.3$ K km/s.

Given the possible initial inhomogeneity of the ambient gas before being swept up and the clumpiness of the outflowing gas, the consistency of the data seems remarkable. Although the data do not allow a precise determination of β, values around 2 arc clearly favored, and values much higher than 4 can almost be ruled out. Since $\alpha + \beta = 2\delta \sim 12$, wc scc that α may take a

value close to 10, and is in general larger than β. We assumed that the CO emission of the shell is optically thin in the above treatment; this may not be a serious problem at higher velocities, but the optical depth will probably increase as velocity offset decreases, and the data points at lower velocities in Figure 4 should be regarded as lower limits. Thus the value of α estimated above should be an overestimate.

3.3 Discussion

α and β are both physically meaningful quantities, as discussed by MC. Assuming power-law forms for $P(\mu)$ and Q(p), MC investigated the behavior of the line profile averaged over the whole outflow, which is equivalent to what is observed with a mall telescope whose beam covers the whole outflow. From this analysis, MC argued that a large value for β and a mall value for α arc required to explain the observational results for the outflows which they analyzed. A large β value implies a substantial density contrast between polar and equatorial directions, which is not observed in studies of dense cores by Myers *et al* (1991) and Fuller & Myers (1 992). A small α implies a poorly collimated wind, which does not explain the existence of optical jets often accompanying molecular bipolar outflows. From these results MC concluded that a '(snow-plow') model with radially directed winds can be ruled out. However, in the case of Mon R2 outflow, it seems that a small value for

β and a large value for α are clearly favored, and the SRLL's "snowplow" model with radially directed winds provides a satisfactory interpretation of the extended blue-shifted emission and the spatial shape of the observed outflow shell. Since the conclusions of MC are drawn under the assumption that the inclination angle i is not too large, while the inclination angle for Mon R.2 outflow is estimated to be $\sim$ 70", a direct comparison] between MC's and our results can not be easily made.

4 Overall Structure of the Mon R2 Outflow

We have so far confined ourselves to the study of the extended blue-shifted emission and the limb-brightened shell caused by the stellar winds directed towards the north-west. An immediate question is: what about the oppositely directed stellar wind from the central source ? Indeed, as mentioned in Section 2, several features are clearly identifiable in the spatial-velocity diagram (Figure 2), and we have only explained the EBL component so far. Meyers-Rice & Lada (1991), devising a paraboloidal shell model with an open end for Mon R2, have decided that the ERL component is the counterpart of the EBL, and attributed the CRL and CBL components to the existence of a second bipolar outflow with axis perpendicular to the EBL-ERL bipolar outflow, though they were puzzled by the obvious Lending of the ERL component (see Figure 11) and Figure '2). What is remarkable is that they

estimated the inclination angle of the EBL-ERL outflow to be $\sim$ 66°, which is consistent with our results, despite the use of a very different shell model. We interpret this as a manifestation of the fact that infered outflow properties are highly sensitive to the inclination angle i.

Several facts together seem to be difficult to understand within this double-bipolar-outflow picture. First, the ERL component appears bent spatially; second, all the components, CRL, ERL, CBL and EBL, have comparable velocity extents; third, the two bipolar outflows have the same center and have axes perpendicular to each other. Although it is not impossible for such two outflows to exist, we feel that it may seem too much a coincidence. Such a doubt is enhanced by the finding by Xie & Goldsmith (1992) that the structure of the Mon R2 GMC is dominated by a large, mainly blue-shifted CO bubble shell which is $\sim$ 30 pc cast-west in extent. These authors have found that the main core region of Mon 1{'2, which harbors the bipolar outflow source, appears to be on the west part of the bubble, moving with a net hluc-shifted velocity of $\sim$ 1 --2 km/s, relative to the $V_{LSR} \sim$ 12 km/s of the ambient gas in the outer part of the GMC. In fact, the core appears to have already become a "peninsula" in the cavity presumably because of the slower velocity it achieves relative to the less dense ambient gas, as can be seen in the velocity channel maps presented in Figure 1. The reality of this peculiar bubble structure of the region is strenthened by the previously reported, puzzling "bent" morphology of the magnetic field in the core (Zaritsky *et al*

1987; Hodapp 1987; Novak *et al* 1989; Aspin & Walther 1990), as discussed by Xie (1992).

How do stellar winds affect the gas in this peculiar, initially inhomogeneous environment ? Conceivably, geometry is again the key. Figure 5 depicts the picture that we have developed so far of the overall structure of the Mon R2 outflow. We think that the development of the stellar winds at one pole directed into the ambient medium to the llortll-west of the cavity gave rise to the EBL component outlined by the limb-brightened shell feature (Figure 1), while the stellar winds at the other pole are directed largely towards the bubble cavity to the east. The first stream of stellar wind towards the north-west (hereafter referred to as NW wind) sweeps up the ambient gas into an elongated shell roughly in the fashion described by SRLL model. If the value of β is close to 2, it means that the: initial condition, as far as the NW wind is concerned, may have been close to a "slab", $p \propto (r\mu)^{-2} \propto 1/z^2$, consistent with the fact that the outflow is located on a bubble shell of large radius approximating a slab. Second, the stellar wind moving towards the south-east (hereafter SE wind) may gradially find increasing difficulty in traveling straight ahead along the polar direction. There could be several effects which influence the development of the SW wind. 1) The density of the gas outside of the very dense core may increase in the SW direction because of the shock compression from the large cavity. As a result, the outflow shell swept up by the initially collimated bipolar stellar winds may achieve a larger velocity

perpendicular to its axis, be forced to develop in the lateral direction, and thus become oblate. This effect can be seen qualitatively from the "snow-plow" modeling discussed in the previous section; a small or a negative β will reduce the major-minor aspect ratio of the outflow effectively (Equation 3); 2) the same effects on the bipolar outflow shell may also be caused by the direct compression from the high pressure of the cavity or the expanding wall of the cavity, as is likely that the bipolar outflow shell driven by the NE wind may be breaking out of the core. Such a compressed outflow shell, if observed with a large inclination angle, would show both red- and blue-slliftccl lobes with the red-shifted lobe possibly larger in extent; and such a pair of blue- and red-shifted lobes, if interpreted as a second pair of bipolar outflow, would also have an "axis" perpendicular to the "first" pair of bipolar outflow, as can be seen in Figure 5.

We have observed a well-s]lapcd bipolar outflow shell in Mon R2. We have found that both the shape of this shell and the mass distribution of high velocity gas as a function of velocity can be satisfactorily explained within the framework of Shu *et al* model. The location of the outflow on a large-scale bubble shell of compressed gas explains the red-blue asymmetry of the outflow and apparent peculiarities in spatial-velocity diagrams,

TX acknowledges Weimin Zhou for very helpful discussions. We thank C. It. Masson, R.L. Snell, and Pat Hartigan for useful comments. This research was supported in part by NSF grant AST 88-15406. The FCRAO telescope is operated with permission of the Metropolitan District Commission. This is contribution 782 of the Five College Astronomy Department.

References

Aspin, C., & Walther, D.M. 1990, *A&A*, 235, 387.

Bachiller, R., Cernicharo, J., Martín-Pintado, J., Tafalla, M. & Lazareff, B. 1990, *AA*, 231,174.

Bally, J. & Lada, C.J. 1983, *ApJ*, 265,824.

Bally, J. & Lane, A.P. 1991, in *The Physics of Star Formation and Early Stellar Evolution*, ed. C. J.Lada and N.D.Kylafis (Dordrecht:K luwer), }).471.

Beckwith, S., Evans 11, N. J., Becklin, E.E., & Neugebauer, G. 1976, *ApJ*, 208, 390.

Cabrit, S., & Bertout, C. 1986, *ApJ, 307, 313.*

Cabrit, S., & Bertout, C. 1990, *ApJ, 348, 530.*

Erickson, N. R., Goldsmith, P.F., Novak, G., Grosslein, R.M., Viscuso, P. J., Erickson, R.B., & Predmore, C. It. 1992, *IEEE Transactions on Microwave Theory and Techniques, 40, 1.*

Fuller, G. A., & Myers, P.C. 1992, *ApJ, 387, 523.*

Hodapp, K.-W. *1987, AA, 172, 304.*

Lada, C.J. 1985, *ARAA, 23, 267.*

Loren, R.B. *1981, ApJ, 2./9, 550.*

Masson, C. R., & Chernin, L.M. 1992, *ApJ,* 387, 1,47 (MC).

Meyers-llicc, B. A., & Lada, C.J. 1991, *ApJ, 366', 445.*

Moriarty -Schieven, G.H. 1988, PhD thesis, University of Massachusetts at Amherst.

Moriarty-Schieven, G.H., & Snell, R.L. 1988, *ApJ, 333,* 316.

Myers, P.C., & Fuller, G. A., Goodman, A. A., & Benson, P.J. 1991, *ApJ, 376,* 561.

Novak, G., Gonatas, D.P., Hildebrand, R.H., & Platt, S.R. 1989, *ApJ,* **345,** *802.*

Shu, F.H., Adams, F.C., & Lizano, S. 1987, *ARAA, 25, 23.*

Shu, F.]]., Ruden, s.] '., Lada, C.J. & Lizano, S. 1991, *ApJ, 370,* L31 (SRLL).

Snell, R.L. *1987, Star Forming Regions, cd.* M. Peimbert & J. Jugaku (Dordrecht:Reidel), 213.

Snell, R,]., Loren, R.B. & Plambeck, R.L. 1980, *ApJ, 239,* L17.

Torrelles, J.M., Rodríguez, L. F., Cantó, J., Carral, P., Marcaide, J., Moran, J.M., & Ho, P.T.P. 1983, *ApJ, 274*, 214.

Wolf, G. A., Lada, C. J., & Bally, J. 1990, *AJ, 100*, 1892.

Xie, T. & Goldsmith, P.F. 1992, in preparation.

Xie, T. 1992, PhD thesis, University of Massachusetts at Amherst.

Zaritsky, D., Shaya, E. J., Scoville, N, Z., Sargent, A.I., & Tytler, D. 1987, *AJ*, 93, 1514.

AUTHORS' ADDRESSES

Paul F. Goldsmith and Nimesh Patel: Five College Radio Astronomy Observatory, 619 Graduate Research Center, Department of Physics and Astronomy, University of Massachusetts, Amherst, MA 01003.

Taoling Xie: Jet Propulsion Lab, MS 169-506, California Institute of Technology, 4800 Oak Grove Drive, Pasadena, CA 91109.

Figure Captions

Figure 1. (a) Channel maps for the $CO\ J = 1 - 0$ emission in the main core region of Mon R2. The central velocity of each 0.65 $km\ s^{-1}$ filter is indicated in the upper left hand corner of each panel. The grey scale ranges from 1 K (white) to 14 K (black). One conspicuous feature in several velocity channel maps with velocity close to the centroid velocity of the core is an eggplant shaped shell extending from the (0, 0) position to NW. (b) An overlay of the shell feature (grey scale) with the high velocity gas (contours). Solid contours are for the blue-shifted emission (V_{LSR} = 2 -- 8 $km\ s^{-1}$) with levels 1, 2, ... 7, 10, 13, ... 22 K $km\ s^{-1}$. The dashed contours are for the red-shifted emission (V_{LSR} = 12 -- 18 $km\ s^{-1}$) with levels 2, 4, ... 26 K $km\ s^{-1}$. The grey scale ranges from 1 K (white) to 14 K (black). (1 c) An overlay of the modeled constant velocity locus with the velocity channel map at 10.8 km/s. The grey scale ranges from 1 K (black) to 14 K (white).

Figure 2. The spatial-velocity diagram along the outflow axis, from (7.5, -10) to (-1 5, 20). We follow Meyers-]{icc & Lada (1 991) in labeling the main features.

Figure 3. (a) Schematic diagram for the outflow shell geometry; (b) Simplified schematic spatial-velocity diagram along the outflow axis at inclination angle i, calculated from the model by assuming infinitely thin shall without

line-broadening.

Figure 4. Mass distribution as a function of the shell velocity for the extended blue-shifted shall. For data points with velocity offsets smaller than 4 km s-l, lower and upper limits arc shown, as explained in text. The solid curves arc model predictions with different values of β.

Figure 5. A cartoon depicting the physical picture of the overall structure of the Mon R2 outflow.

Fig 1a

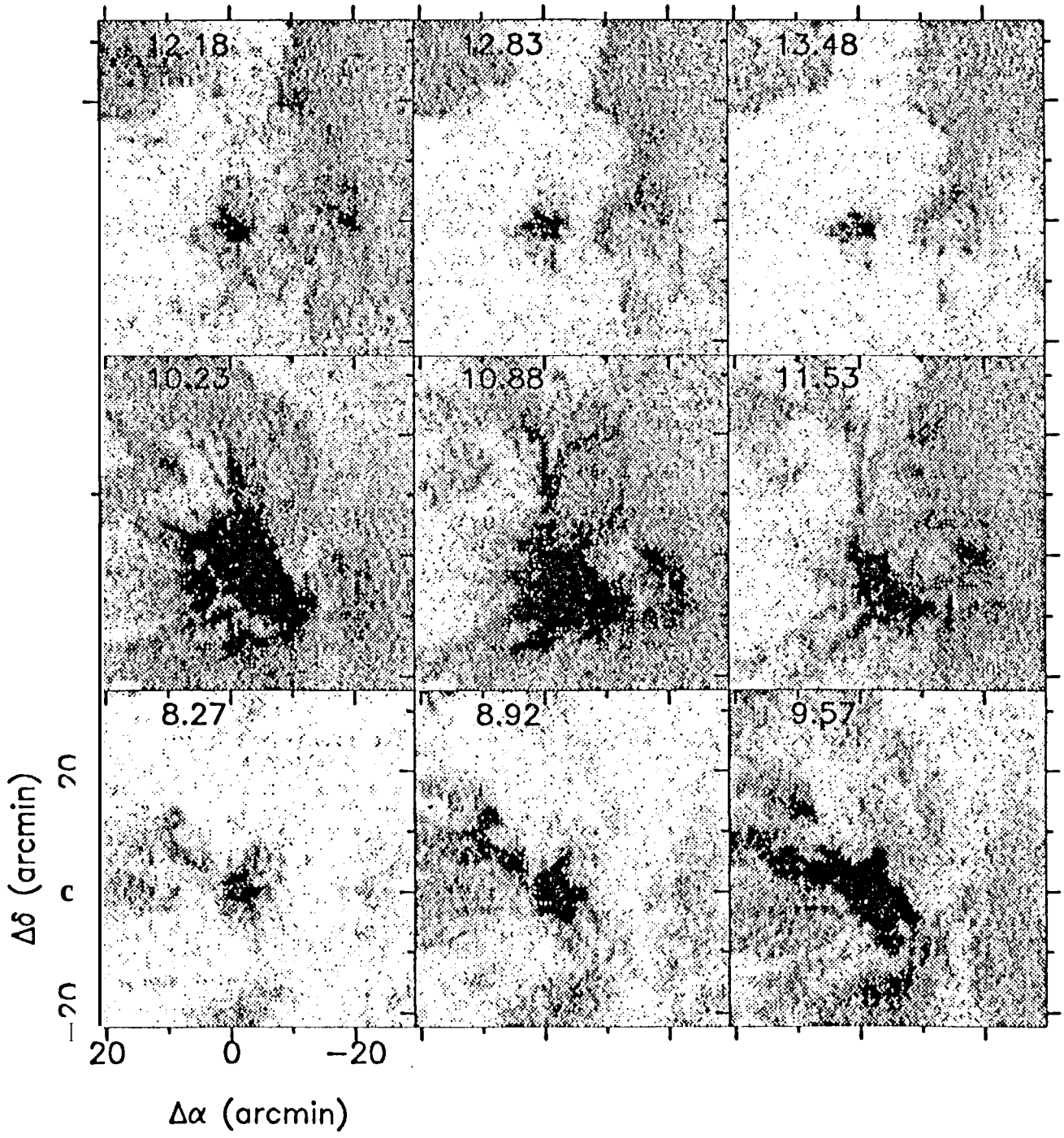
12.18
12.83
13.48
10.23
10.88
11.53
8.27
8.92
9.57
20
0
−20
Δδ (arcmin)
Δα (arcmin)

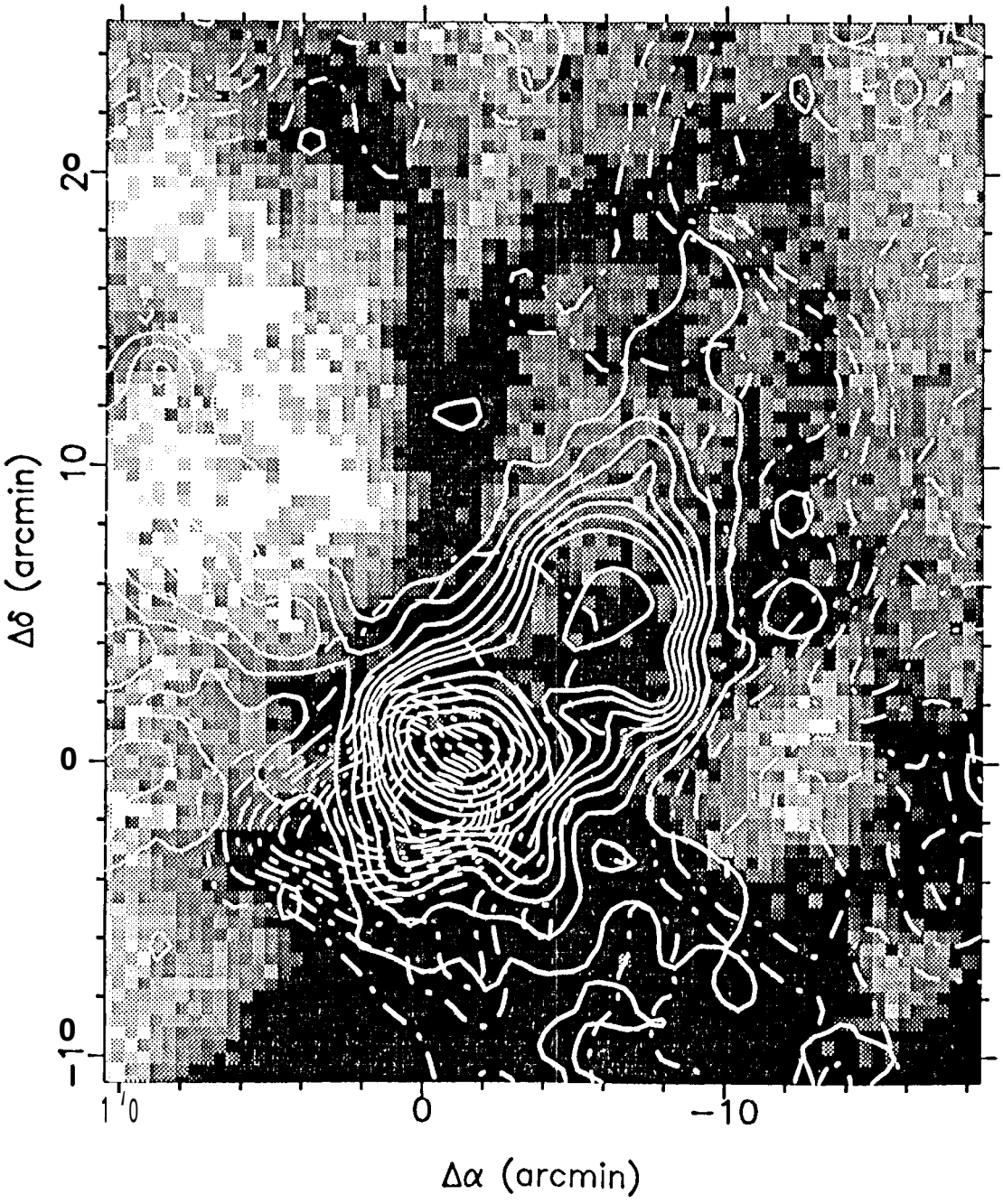
2°
10
0
−10
Δδ (arcmin)
10
0
−10
Δα (arcmin)

Fig 1c

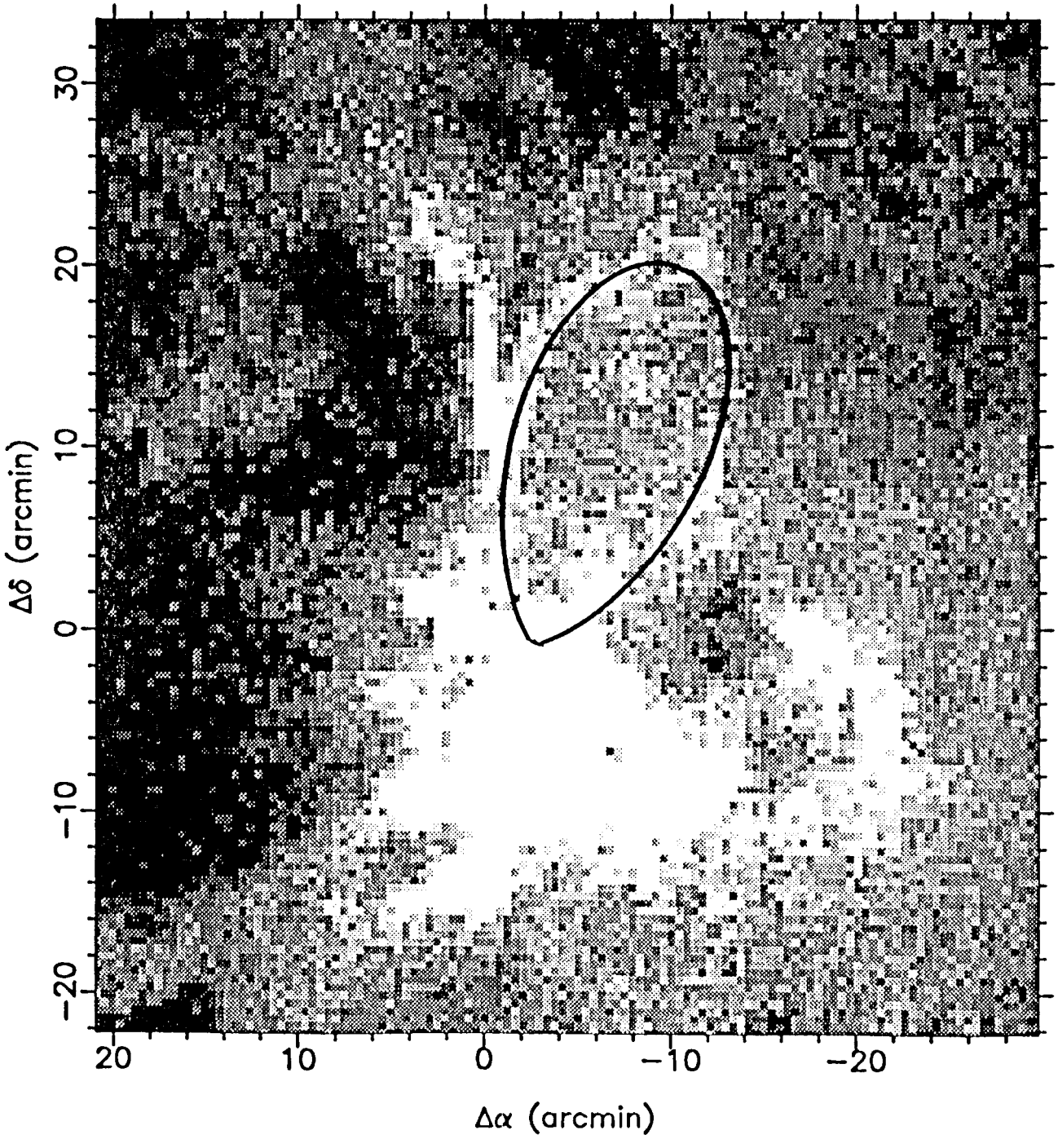

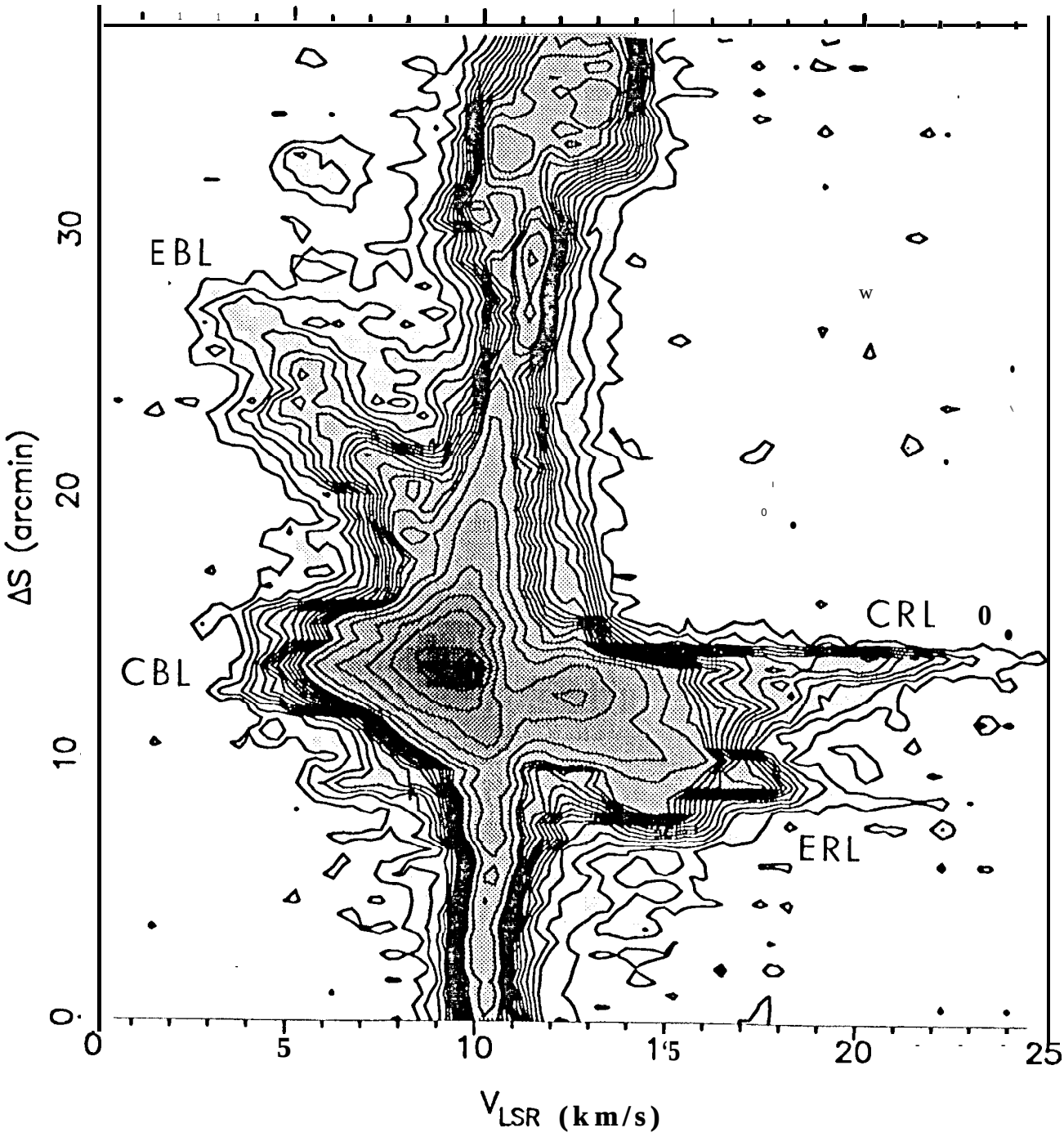
EBL
CBL
CRL
ERL
W
0
ΔS (arcmin)
0
10
20
30
0
5
10
15
20
25
V_LSR (km/s)

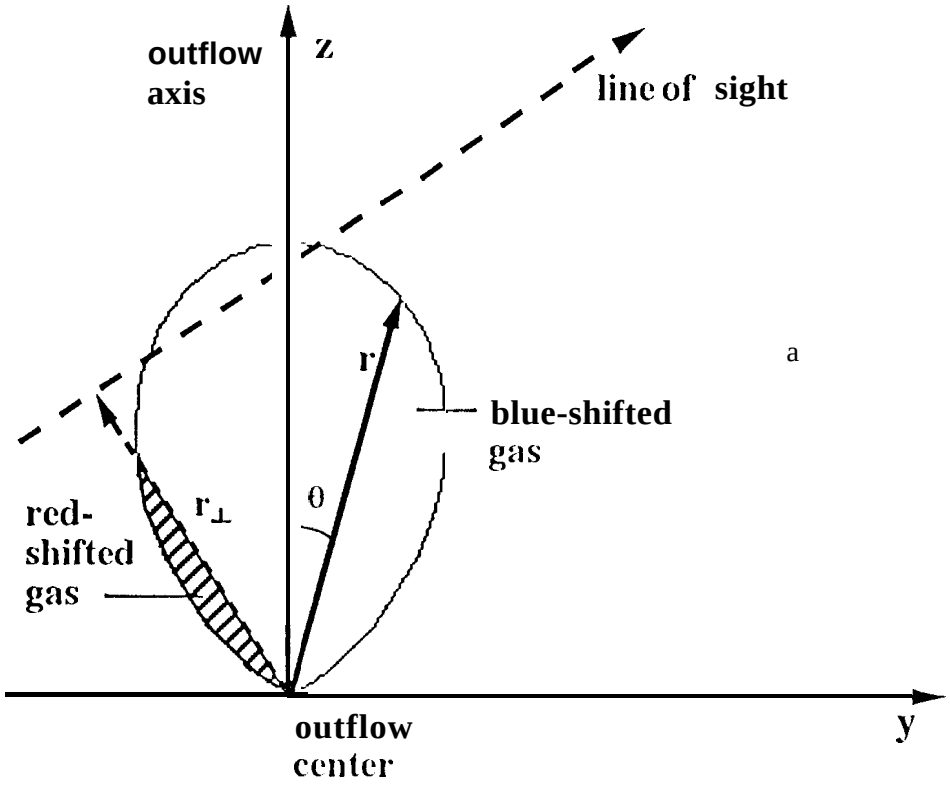
outflow
axis
z
line of sight
r
blue-shifted
gas
red-
shifted
gas
$r_\perp$
θ
outflow
center
y

a

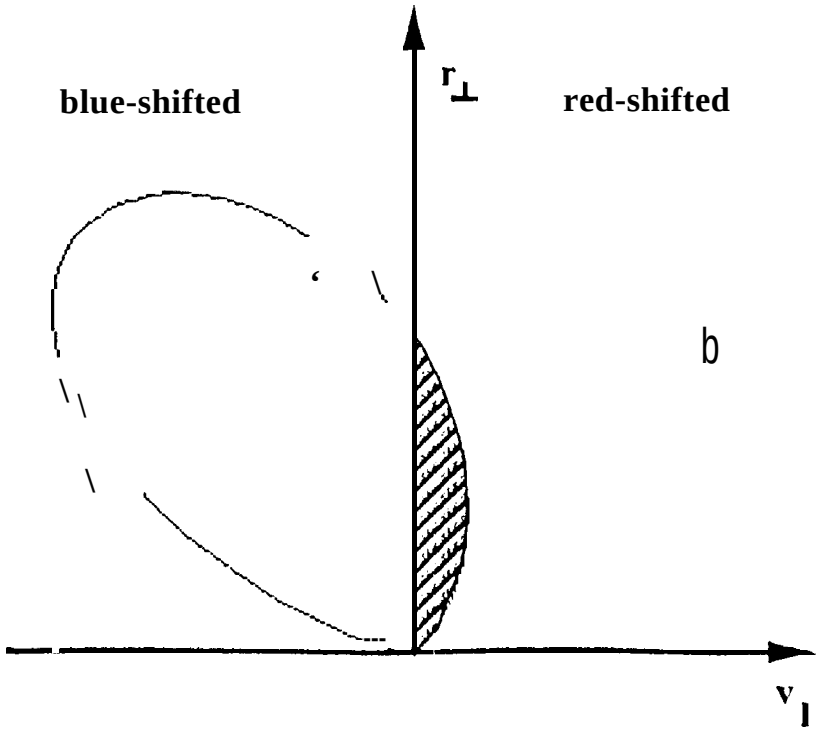
blue-shifted
$r_\perp$
red-shifted
v_l

b

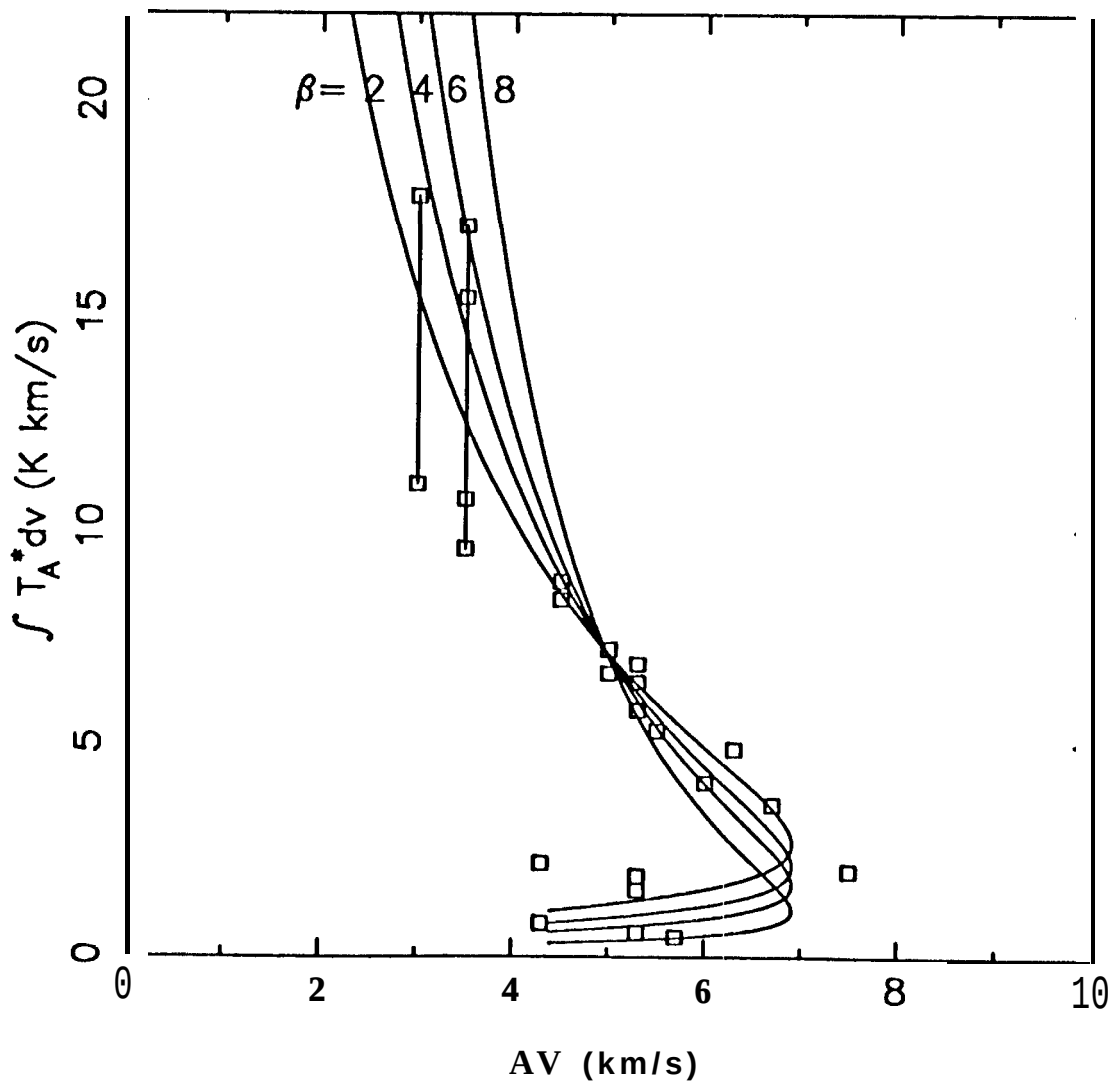
β= 2 4 6 8
∫ T_A* dv (K km/s)
AV (km/s)
0
5
10
15
20
0
2
4
6
8
10

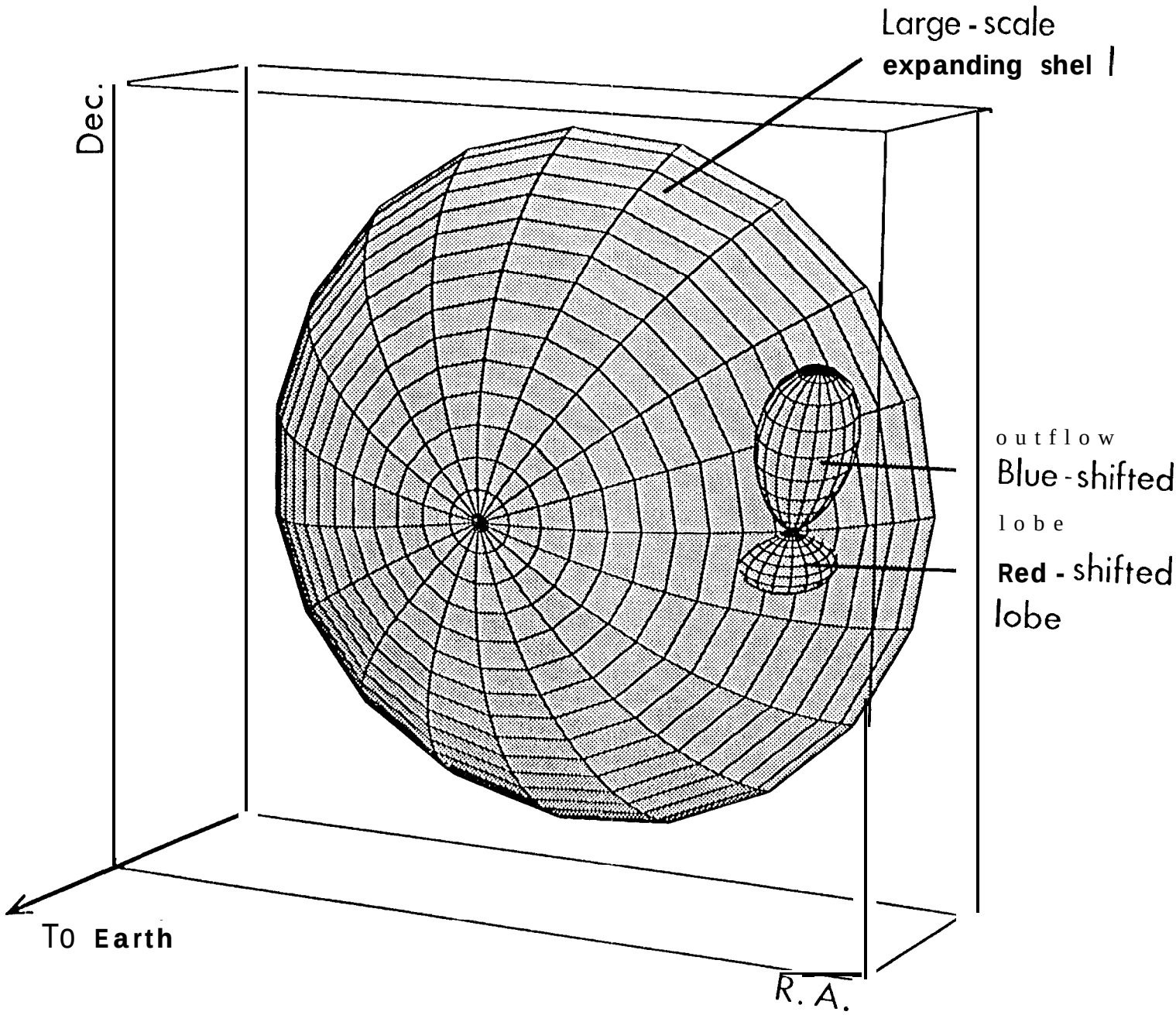
Large - scale
expanding shel l
Dec.
outflow
Blue - shifted
lobe
Red - shifted
lobe
To Earth
R. A.